The monitoring network of greenhouse gas (CO$_2$, CH$_4$) in the Paris' region

Josselin Doc[1], Michel Ramonet[1], François-Marie Bréon[1], Delphine Combaz[2], Mali Chariot[1], Morgan Lopez[1], Marc Delmotte[1], Cristelle Cailteau-Fischbach[3,4], Guillaume Nief[1], Nathanaël Laporte[1], Thomas Lauvaux[1,5], Philippe Ciais[1]

[1] Laboratoire des Sciences du Climat et de l'Environnement (LSCE-IPSL), UMR CEA-CNRS-UVSQ, Gif-sur-Yvette, France

[2] Groupe d'Étude sur les Géomatériaux et ENvironnements Anthropisés (GEGENA), URCA, Reims, France

[3] Laboratoire ATMosphères, Observations Spatiales (LATMOS), Sorbonne Université - Campus Pierre et Marie Curie, Paris, France

[4] Sorbonne Université, CNRS, UAR 3455, OSU Ecce Terra, Paris, France

[5] Groupe de Spectroscopie Moléculaire et Atmosphérique (GSMA), UMR CNRS-URCA, Reims, France

Correspondence to: Josselin DOC (josselin.doc@lsce.ipsl.fr)

Abstract. There is a growing interest for the study of greenhouse gas emissions over urban areas. In this context, a network for measuring greenhouse gas concentrations was set up in Paris in 2015. Since then, seven stations located in and around Paris and equipped with cavity ring-down spectrometers (CRDS) have been monitoring gas concentrations of different species (CO$_2$, CH$_4$, CO) on a continuous basis. Procedures for maintenance, calibration, data processing have been adapted to ensure that the network is operational, providing good quality data in near-real time (NRT) and with high availability. The CO$_2$ and CH$_4$ concentrations show a growth rate of the baseline (linear trend of the averaged concentrations over the Paris region) concentrations (+2.34 ppm CO$_2$/year and +11.1 ppb CH$_4$/year) between 2015 and 2022 consistent with that observed at remote observatories such as Jungfraujoch (Switzerland). The amplitude of the CO$_2$ seasonal cycle is around 20 ppm (i.e. around 5%) while that of CH$_4$ is 40 ppb (i.e. around 2%). The concentration gradients calculated as the differences between up- and down-wind concentrations, can be used to infer the emissions for long lived species. We use the measurements from the 100m Saclay tower, outside of Paris, as a regional background during suitable wind direction conditions. The largest differences with these background measurements are observed in the two stations that are located within Paris (JUS and CDS), with urban offset up to ~50 ppm CO$_2$ and ~100 ppb CH$_4$ in winter and ~10 ppm CO$_2$ and ~50 ppb CH$_4$ in summer. In winter, the co-variability of CO and CO$_2$ hourly measurements (correlation coefficient r ~ 0.9 in all stations) indicates that the concentration variability is driven by anthropogenic emissions. Conversely, in summer, lower correlations between these

30   two gases concentration (r ~ 0.3 in peri-urban stations and r ~ 0.6 at CDS and JUS) shows the more dominant role of vegetation fluxes.

1. Introduction

Carbon dioxide (CO_2) and methane (CH_4) are the main greenhouse gas (GHG) emitted in urban areas by anthropogenic activities, such as road traffic, energy production, industry or residential heating. Urban areas cover around 3% of the Earth's
35   surface (*Liu et al.* 2014), are home to 56% of the population (World Bank based on data from the UN Population Division, 2023) and account for an estimated 70% of global CO_2 emissions (IPCC, 2022), mainly driven by traffic and residential sectors. Although not a significant GHG, Carbon monoxide is a pollutant co-emitted together with CO_2 during combustion reactions. In cities, it can then be used as a tracer of anthropogenic GHG emissions. Urban atmospheric GHG measurement networks have been deployed in few cities (*Mitchell et al.* 2022, *Verhulst et al.* 2017, *Gonzalez Del Castillo et al.* 2022,
40   *Dietrich et al.* 2021, *Pugliese et al.* 2018, *Shusterman et al.* 2016, *Lian et al.* 2024, *Lauvaux et al.* 2020) for estimating emissions based on a methodology referred to as atmospheric inversions. Here we present eight years of high precision continuous measurements of CO_2, CH_4, and CO concentrations across a network of seven ground-based stations located around and inside the city of Paris. With a total population of 12 million inhabitants (2.1 million in the Paris' city-center only) and estimated annual emissions of 37 Mt (4.78 Mt in the Paris' city center only) CO2eq in 2021 (AIRPARIF, 2024),
45   dominated by traffic and residential and commercial heating, Paris and its urban area are well suited to setting up such a network. The interest in the urban area of Paris is reinforced by its geographical isolation. Unlike other European cities, it is surrounded by more rural areas, which makes it easier to interpret the concentration measurements in terms of emissions. The monitoring network in Île-de-France was started in late 2014 with two stations and reached seven stations in 2017 (*Bréon et al.* 2015, *Staufer et al.* 2016, *Xueref-Remy et al.* 2018, *Lian et al.* 2021, *Lian et al.* 2022, *Nalini et al.* 2022, *Lian et*
50   *al.* 2023). With the objective of estimating the urban area emissions, the observation strategy is to make measurements at peri-urban locations both upwind and downwind along the prevailing wind direction. The analysis of weather data shows that the wind direction is predominantly from the South-West (23 %) or the North-East (13 %) sectors (over eight 45° sectors: N, NE, E, SE, S, SW, W, NW). The spatial distribution of the stations along the axis of the prevailing wind allows the calculation of the CO_2, CH_4 and CO downwind minus upwind gradients. Part of the advantage of setting up such a
55   network is to monitor the atmospheric gradients along the trajectories of air masses, and use this information in an inverse modelling process to estimate surface emissions. In the following we present the instruments and stations set up, calibration process and measurement accuracy. We then summarize the time series and temporal gaps due to instruments malfunction. We analyze the time series of CO_2, CH_4 and CO and derive their seasonal and diurnal cycles, as well as their variations as a function of wind direction and speed.

2. Presentation of the measurement sites and instruments involved in the monitoring network

2.1. One network, seven measurement sites

The measurement network of greenhouse gases in Île-de-France region is composed of seven stations: the two first stations (OVS and COU) have been set up in 2014 and the last one (GNS) has been set up in 2017. CDS and JUS stations are considered as "urban sites" due to their location inside the Paris city. The five remaining sites are located around Paris and are called "peri-urban sites" (Fig. 1). Among these, Saclay (SAC) station is part of the European ICOS network (*Heiskanen et al.* 2022).
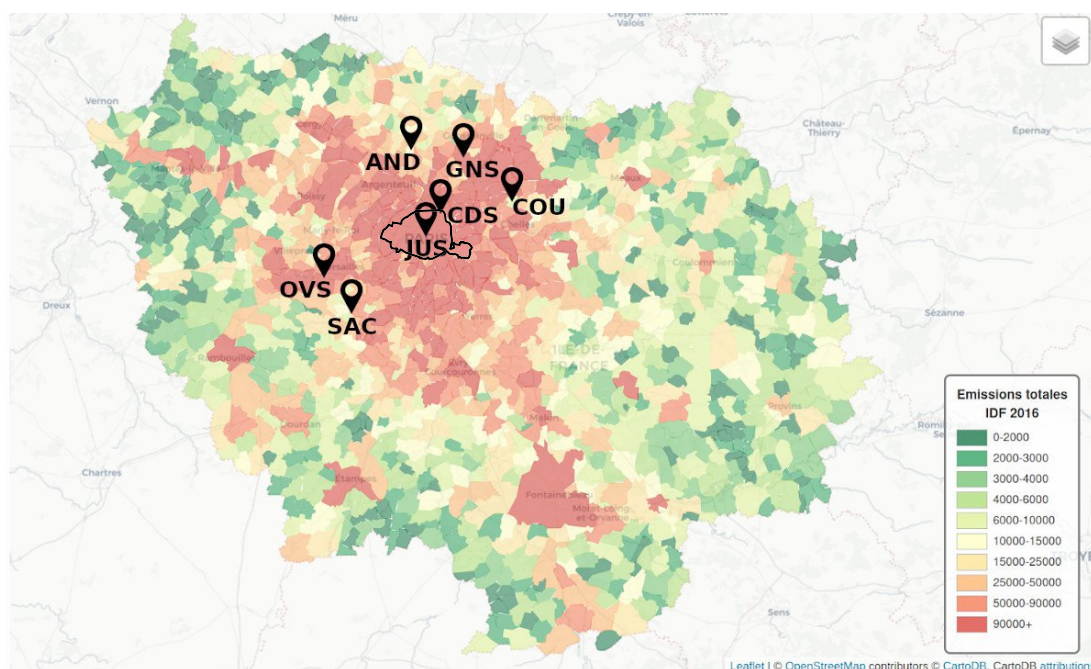
Figure 1. Location of the greenhouse gas measurement sites of the Parisian network in the Île-de-France region (colored area). The black line shows the Paris city border

More information such as the precise location, air intake's height or the altitude of the station are provided in Table 1.

Site	Latitude	Longitude	Ground level's altitude above sea level (m)	Air inlet altitude above ground level (m)
AND	49.0126	2.3018	175	60
CDS	48.8956	2.3880	45	34
COU	48.9242	2.5680	126	30
GNS	49.0052	2.4205	81	36
JUS	48.8464	2.3561	38	30
OVS	48.7779	2.0486	150	20
SAC	48.7227	2.1420	160	15, 60, 100

Table 1. Location of each site from the Parisian network, station level above sea level and air inlet altitude above ground level.

Below is a short presentation of the seven sites in the Paris region:

- Cité des Sciences (CDS): located in the North-East of Paris, beside the ring road that goes around the city, the GHG analyzer was set up in the Science Museum on the occasion of COP-21 held in Paris in 2015. The air intake is placed on top of the building, 34 meters above ground level.

- Jussieu (JUS): located in the center of Paris, has been in operation since September 2016 within the Sorbonne University campus located in a densely urbanized area. The air intake is placed on the roof of the building, right above the laboratory where the instrument is placed, at 30 meters above ground level. It is part of the QUALAIR instrumented platform, and is co-located with the TCCON station in Paris (Té et al., 2016).

- Andilly (AND): located 17.8 kilometers in the North of Paris, in an area mainly covered with forest. This station has been in operation since July 2015. The instrument is placed in a tall tower primarily used for television broadcasting. The air intake is placed on top of the tower, at 60 meters above ground level. Potential pollution sources in the area include a waste processing facility, 1.4 kilometers north of the measurement site.

- Coubron (COU): located in the country side, 17.3 kilometers north-est of Paris' center, this station has been in operation since July 2014. The surrounding area is mostly covered by forest with a few towns. The air intake is placed on top of a radar tower used for civil aviation, at 30 meters above ground level. Potential local sources in the area include an industrial waste treatment plant 2.7 kilometers East and the Charles-de-Gaulle airport 9.2 kilometers North of the measurement site.

- Gonesse (GNS): located 17 kilometers north-north-east of Paris city center in a residential area, this station has been in operation since June 2017. The air intake is placed on top of a water tower, 36 meters above ground level. A landfill and waste treatment facility is located 2.5 kilometers north of the site. Two airports are also located in the vicinity of the site: Charles-de-Gaulle, 8 kilometers east and Le Bourget (smaller airport, mainly used by private jets), 4.5 kilometers south-south-east.

- Observatoire de Versailles – Saint-Quentin (OVS): located 24 kilometers south-west of Paris' center, this station is surrounded by a residential area, this station have been in operation since August 2014. The air intake is placed on the roof of the laboratory's building, 20 meters high above ground level. Measurements data analysis have shown that the building itself, with several exhausts from the building's boiler and various experiments conducted at the observatory, may be a significant contribution to the measurement variability.

- Saclay (SAC): located 21 kilometers south-west of Paris' center, in a mostly rural area, this station works since July 2015. Three air intakes are placed on a 100 meters tower at 15 meters, 60 meters and 100 meters above ground level (agl). There are two heat gas plants in the vicinity of the site (800 meters away), used for heating at the cold period. Weather measurements (wind speed, wind direction, temperature, relative humidity, pressure) used in our work are made at 100 meters. This station was approved as part of the ICOS research infrastructure in 2020, and now follows the network's measurement protocols (*Yver-Kwok et al.* 2021). The tower also hosts wind

measurements at 100 m above ground level which are used here for the interpretation of the concentration measurements at the regional scale.

2.2. Instruments

Each of the 7 sites is equipped with a Cavity Ring-Down Spectroscopy (CRDS) instrument (Picarro G2301 or G2401)
110 measuring two or three species (CO_2, CH_4, CO). The instrument's pump samples the air through a line with an outer diameter of ¼ inch (Synflex Dekabon tubing). The sampling head can be placed dozens of meters away from the instrument, generally on top of a tower or building. A 2 µm particulate filter is installed on the sampling line in order to protect the instrument's cavity from dust and particles. At all the sites except JUS and SAC, the instruments are calibrated every 6 months with the same 3 calibration cylinders that are moved to each site periodically. These cylinders are filled with
115 synthetic air, and their concentrations ranges from 371 ppm to 504 ppm for CO_2, 1646 to 2082 ppb for CH_4, and 81 to 492 ppb for CO. JUS station has its own calibration scale, also composed of three cylinders, permanently installed on the site, and the calibration is performed every 6 months. In between two calibrations, a reference gas is measured once a day in order to apply a one-point calibration and correct for short term drifts. A target gas is also analyzed once a day to evaluate the bias and repeatability of the time series.

120 All the cylinders used on the Parisian network are calibrated at LSCE central laboratory before being sent to the sites. The calibration is performed on a reference instrument (Picarro G2401) against a WMO-NOAA scale composed of six cylinders with concentration varying from 368.75 to 516.57 ppm for CO_2, 1724.9 to 2548.9 ppb for CH_4, and 140.8 to 492.1 ppb for CO. All data are therefore expressed in the current reference scale: WMO-X2019, WMO-X2004A, and WMO-X2014A respectively for CO_2, CH_4 and CO. The uncertainties in the concentrations of CO_2, CH_4 and CO in the calibration cylinders
125 for this scale are provided by NOAA and are 0.01 ppm CO_2, 0.1 ppb CH_4 and 0.4 ppb CO (*Hall et al.* 2023). We estimate the uncertainty in the calibration of the instruments at the different locations to be less than 0.1 ppm CO_2, 1 ppb CH_4 and 2 ppb CO.

At SAC station (class 1 ICOS station) the setup is different in order to comply with ICOS protocols. Two CRDS analyzers are permanently installed, measuring CO_2, CH_4 and CO. Synflex sampling lines are installed on the tower at three different
130 heights: 15 meters, 60 meters and 100 meters. One instrument samples continuously the air only from the 100 meters line, while the other one samples alternatively from the three lines, switching height every ten minutes. The calibration (according to the ICOS standard procedures described in *Yver-Kwok et al. 2021*) is performed once a month on every instrument, using four gas cylinders provided by the ICOS Flask and Calibration Laboratory in Jena, with concentrations varying from 368 ppm to 447 ppm for CO_2, 1700 ppb to 2300 ppb for CH_4, and 67 ppb to 1013 ppb for CO.
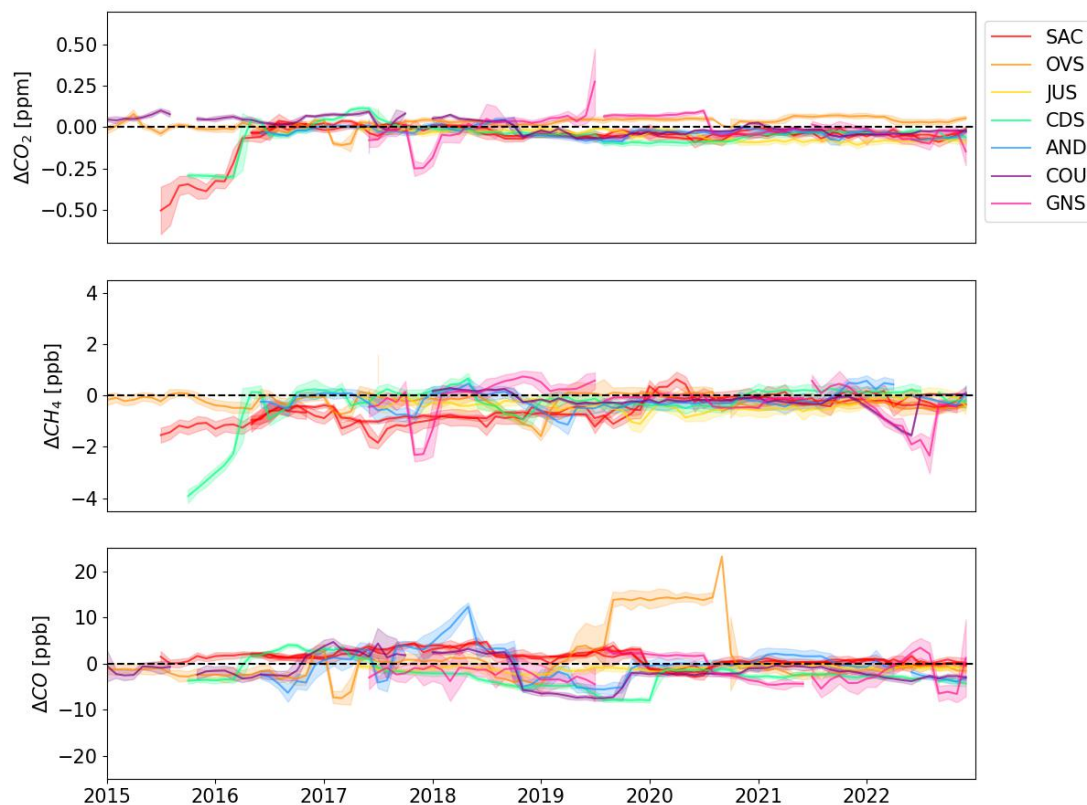
135

Figure 2: Monthly means of the differences between target gas measurements and assigned values of the tanks during the daily injections in all the stations of the Parisian network, from 2015-01-01 to 2022-12-31.

While six-monthly calibrations can correct long-term instrument drift, it is the daily injections of the reference gas (air with known and recorded concentrations of the species under study) that can correct for short-term drift. Fig. 2 shows the monthly

140 averages of the differences between the concentration values measured during the daily target gas injections on site, and the expected values from the target gas. Ideally, the difference should remain close to 0. Since target gas is injected at a multi-position valve, it cannot be used to check drifts arising from the entire air sampling line. It is important to bear in mind that only the downstream part of this valve is evaluated by the target gas. It is also important to note that target gas measurement bias can be attributed either to the analyzer, to the air sampling line shared with the target gas line, or to the target gas

145 injection. For CO_2, the differences between measurements and assigned values remain within +/- 0.1 ppm (i.e. approximately 0.025% of the atmospheric concentration) for 89% of the daily injections. Two stations (SAC and CDS) showed greater biases in 2015 and early 2016. This corresponds to their first few months of operation, and the most likely explanation is insufficient flush of the pressure regulators used for the target gases at these stations, which would mean that ambient air measurements would not be affected. CH_4 measurements are also fairly constant and show fairly small deviations from the

150 reference value at all the stations. These deviations are around 1 to 2 ppb, or about 0.1% of the mean concentration in the atmosphere. Over the same period as for CO_2 (until early 2016), the CDS and SAC stations show a higher bias. Once again,

the bias for these stations is very much reduced once the stations are commissioned. CO target biases are slightly more variable. The differences between the measurements and the assigned value range from around -5 to 5 ppb, which is about 5% of the typical atmospheric concentration. Between September 4th, 2019 and October 7th, 2020, CO measurements are

155 biased at the OVS station for unknown reasons. As the bias is nearly constant over the period (14.1 ± 1 ppb), its mean value has been used to correct the atmospheric measurements, and an additional uncertainty is set over this period.

3. Data coverage and identification of local contaminations

3.1. Data coverage

The Paris' greenhouse gas monitoring network is involved in different national and European research projects, in particular

160 the ICOS-Cities project (*Christen et al.* 2023). In this context, one of the objectives is to demonstrate our ability to carry out continuous measurements with the fullest possible temporal coverage. A data processing and automatic quality control system makes the results available in near-real time (NRT, 24hr). Fig. 3 shows the daily data availability, defined as : $A = 100*N_d/N_{max}$, where A is data availability, N_d is the number of valid data items in a day after quality control, and N_{max} is the maximum number of data items that could be available in a day (e.g. 24 in the case of hourly data).

165

Figure 3. Data availability, averaged on a monthly time scale, in all stations in the Paris' network from 2015-01-01 to 2023-12-31.
Since the three species are measured by the same instrument, data availability is similar for all species measured at a given station and the figure is not broken down by species. Nevertheless, there may be minor differences between the availability of data for different species, as a result of quality control carried out retrospectively. While some stations were already

170 operational at the beginning of 2015 (OVS and COU), others were installed later, until 2017 (GNS). Once the stations are operational, the data availability rate is generally higher than 90%, which illustrates the positive impact of the maintenance

work carried out on the network. The SAC station is unique in that it has three measurement levels (15, 60 and 100 meters) and two distinct instruments. One instrument measures continuously at 100 meters. The second measures alternately at 15, 60 meters, and 100 meters. This explains the particularly high data availability at SAC 100 (SAC_{100}) meters and the similar
175   availability at 15 and 60 meters. In 2019, the apparatus for shifting between the 3 sampling heights was out of order, which explains the data gaps at 15 and 60 m only. The few differences between data availability at these two levels (15 and 60 meters) can be explained by data rejected during quality control and by technical failures that are not linked to the instrument itself, but rather to the inlet lines.

The high data availability allows a meaningful analysis of the concentration variability and trend. One-off events, such as
180   pollution peaks when weather conditions prevent the dispersion of locally emitted gases, or the appearance of plumes from elsewhere (e.g. the passage of a plume from fires in south west France in summer 2022), can be rapidly observed and documented. The data from such an urban network can also be used to feed modeling work to better study the impact of cities on the climate and/or to quantify the impact of emission reduction measures taken by political decision-makers. In addition, monitoring the availability and quality of data in near real time means that any instrument failure can be detected
185   and dealt with quickly.

3.2. Identification of the spikes in all stations

In-situ measurements sometime show very short-lived peaks, which are not representative of longer term time series. A filtering method developed for ICOS atmospheric stations, analyzes the high-frequency variability of minute data, enabling automatic identification of these measurements as "spikes" (as described in *El Yazidi et al.* 2018 and *Cristofanelli et al.*
190   2023). In the followings, this filter will be referred to as the 'statistical filter'. Another filter is used for the GNS and OVS stations to cope with the well-identified local source of contamination. This filter, presented in section 3.3, is based on the criteria of wind speed and direction and the variability of the measurements. It will be referred to as the 'wind sector filter'. Fig. 4 shows mean differences between hourly measurements with and without spikes as a function of local time.
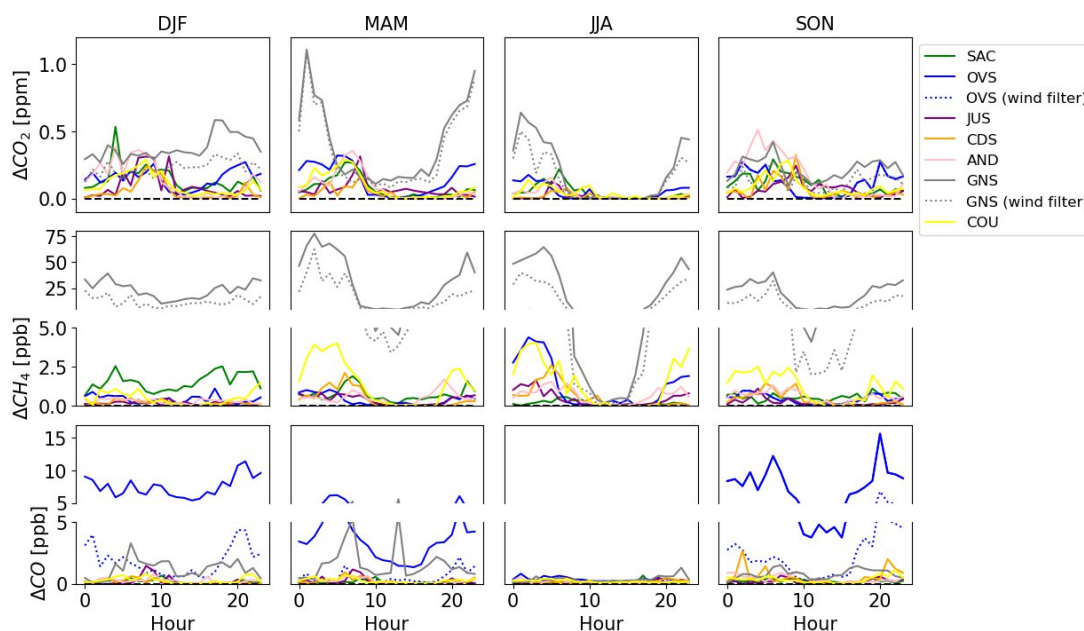
Figure 4. Diurnal cycles of the hourly mean concentration reduction when applying the statistical spike filter. The dotted lines are for the specific wind sector filter at OVS and GNS. Data are aggregated by three-month seasonal periods (DJF for winter, MAM for spring, JJA for summer and SON for autumn).

Fig. 4 shows that the impact of spike filtering is larger in winter for CO_2 and CO, with mean concentration reduction of around 0.2 ppm CO_2 and 1 ppb CO. For methane, the impact is similar from one season to the next. As for the diurnal cycle, irrespective of the season, the impact of spike filtering is greater at night than during the day, reflecting the lower dilution of air masses during the night and therefore a greater likelihood of being influenced by local sources.

Three singular behaviors can be observed:

- The SAC station shows a high impact of methane spikes in winter.This is due to a well identified contamination from the campus' heating plant. This is why it is only present in winter, when the wind is coming from North-East sector.

- The impacts of methane spikes are larger at GNS station (up to 75 ppb). A waste disposal site located 3 km north of the station has been identified as the source of methane contamination.

- CO spikes have a major impact on the OVS station.This time, it's on the roof of the building itself that the local sources have been identified. In fact, several chimneys are present, evacuating gases used in experiments in the building's laboratories, as well as combustion gases from the site's heating system. For this reason, filtering these spikes has a significant effect for most of the year. The slight difference between measurements with and without spikes in summer can be explained by the fact that no heating system is used, and by the fact that fewer experiments are carried out during this period (and therefore fewer gases are released).

3.3. Identification of local contamination in GNS and OVS stations

215   Despite the statistical filter, based on high frequency data variability, that is applied on all stations, the GNS and OVS sites appear to be particularly impacted by local sources, which justifies an additional selection based on wind sectors.

a) OVS   b) GNS
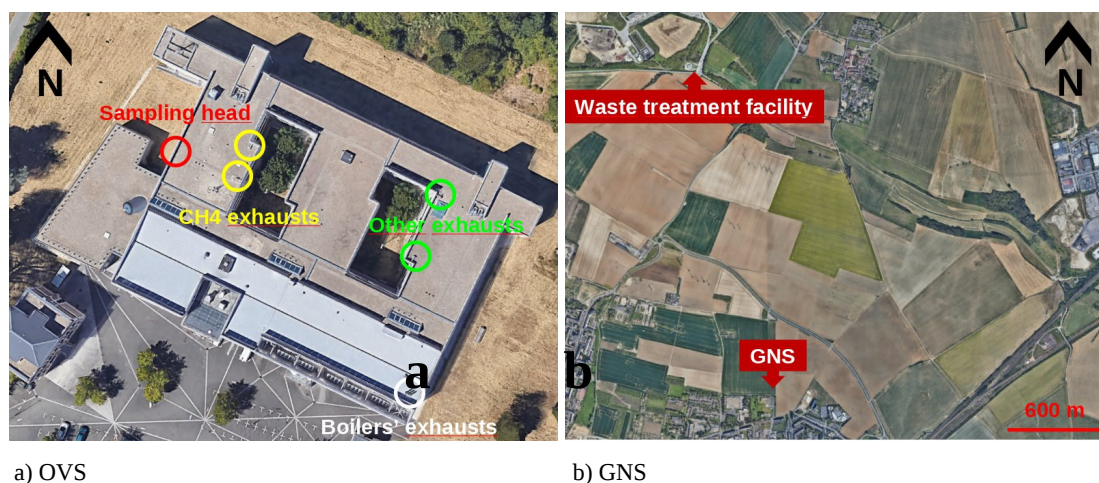
Figure 5. Aerial views of OVS (a) and GNS (b) stations with identified contamination sources that necessitate data filtering based
220   **on wind direction. ©Aerial views: Google Earth.**

The main contamination sources are located 3 kilometers north of GNS station (waste treatment facility) and on the building itself in OVS station (laboratory exhausts), see section 2. As a consequence, a data filtering using an algorithm based on the wind speed and direction and the trace gas concentration variability, (Table 2) is applied on hourly data. The hourly data identified as polluted with this filter are classified as "local air-masses" and are not used for the long-term regional analysis.

225   They are based on three criteria determined empirically by comparing measurements from these stations with measurements from the nearest stations:

- Wind direction from contaminating spots
- Low wind speed
- The large standard deviation of minute data over one hour periods

Local filters in OVS and GNS stations		
Parameter	**OVS**	**GNS**
Wind direction (°)	WD <= 200	WD <= 75 or WD >= 260
Wind speed (m.s^{-1})	WS < 3	WS < 4
STD (ppm or ppb)	CO_2 ➜ STD > 3 ppm	CO_2 ➜ STD > 3 ppm
	CH_4 ➜ STD > 10 ppb	CH_4 ➜ STD > 10 ppb
	CO ➜ STD > 10 ppb	CO ➜ STD > 10 ppb
Contaminated hourly data	CO_2 ➜ 8.87 %	CO_2 ➜ 5.28 %

(%)	CH$_4$ ➜ 9.03 %	CH$_4$ ➜ 14.15 %
	CO ➜ 13.23 %	CO ➜ 8.68 %

230

Table 2. Parameters used for the wind sector filtering in OVS and GNS stations. They have been determined empirically by comparing the measurements in OVS and GNS stations to the measurements in the closest stations. All three criteria must be met for the measurement to be classified as "local".

This wind sector filter only applies to the GNS and OVS stations because of the clearly identified sources of pollution near
235 these sites. The SAC station also has a well-identified local source of pollution: the chimney of the campus heating plant. We could apply the same wind-based filter and determine the criteria by comparison with the nearest station (OVS), but it seems that the statistical filter is sufficient for this station. In this study, we will use hourly data to which we have applied the filter based on high-frequency measurement variability for all stations (section 3.2), and to which we have added the wind sector filter for GNS and OVS stations (section 3.3), between 2015-01-01 and 2022-12-31.

240 Fig. 4 also shows, in dotted lines (for CH$_4$ at GNS and CO at OVS stations), the impact of the local source filtering on the concentration mean daily cycle. The impact of the wind sector filter differs between the two stations. In GNS station, the impact of the statistical spike filter and that based on the wind sector are very similar. On the contrary, the effect seems different at OVS station. Indeed, the difference between hourly measurements with and without statistically filtered spikes after removing data identified as local by the wind sector filter is very similar to other stations in all seasons. This means that
245 contaminations are almost all identified by the wind sector filter. We hypothesize that this results from the short distance between the sources and the analyzer's air inlet. At GNS station, about three kilometers separate the landfill from the station, whereas at OVS station they are only a few meters apart. Emissions are more diluted in the contaminated air mass at GNS station so that their impact on the concentration is temporally smooth which makes them less easily identifiable than at OVS station.

250 The data rejected by these two filters due to local contamination are not taken into account in the analyses presented in this article, even though they are valid measurements.They can therefore be the subject of specific studies, for example to quantify CO$_2$ or CH$_4$ emissions from a clearly identified hot spot located within a few km from the monitoring station.

4. Time series

4.1. Eight years of measurements across the Paris region

255 Concentration measurements are presented in Fig. 6 over a period of up to eight years (depending on when the station was commissioned). These measurements are used to carry out statistical analysis of the trend and variabilities of the CO$_2$, CH$_4$ and CO concentration measurements. In this study, we will focus on the daily and annual cycles.
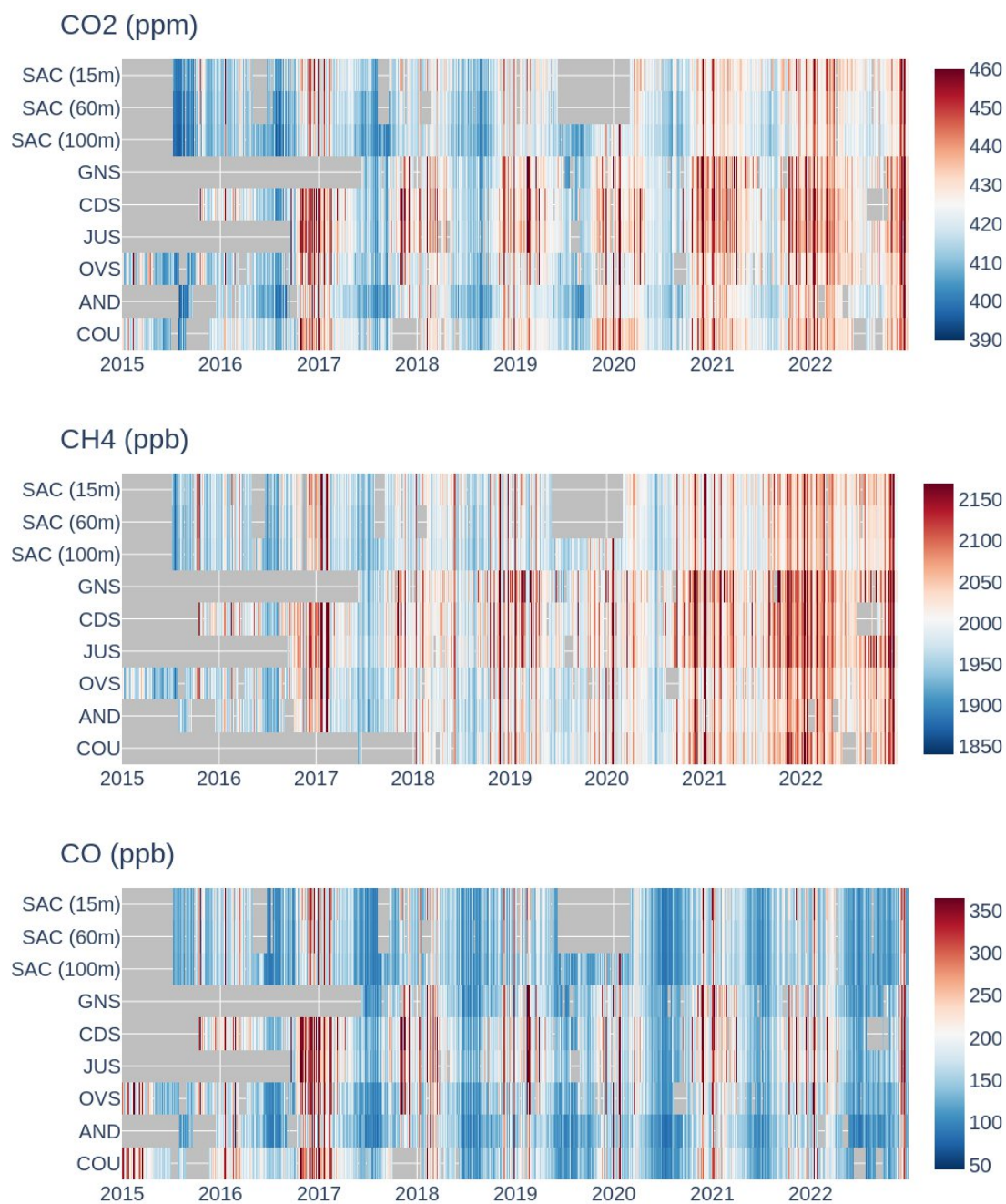
Figure 6. Time series of the daily averages of CO₂, CH₄ and CO concentrations in the Parisian network from 2015-01-01 to 2022-12-31.

Fig. 6 shows the time series of daily averages of CO₂, CH₄ and CO concentration measurements at all the stations in the Paris network. The CO₂ measurements clearly show a seasonal cycle with a maximum in winter and a minimum in summer.

265 The amplitude of the seasonal cycle is around 20 ppm. When averaged over the 7 stations, the data set also shows a mean trend of 2.3 ppm/year over the last eight years. This is in line with the global trend as indicated by 'background' measurements at the Mauna Loa observatory (Hawaii) over the same period (https://gml.noaa.gov/ccgg/trends/gr.html) and Jungfraujoch observatory.

CH_4 measurements also show an increasing trend over the eight years of the study (+11 ppb/year). The CH_4 seasonal cycle is
270 not as visible as in the case of CO_2, because the day-to-day variability is proportionally higher than that of CO_2, and therefore makes the seasonal cycle more difficult to identify. Quantifying the contributions of the various sources and sinks to the seasonal cycle is more complex for CH_4 than for CO_2. Both gases are subject to the same atmospheric dispersion processes, with more intense mixing in the boundary layer in summer than in winter. On the other hand, exchanges with the terrestrial biosphere, which strongly dominate seasonal CO_2 fluxes, are not dominant for CH_4 in the Paris region. CH_4
275 emissions are less cyclical and more homogeneous throughout the year. On the other hand, methane is mostly destroyed by photochemistry, which is more effective in summer than in winter. Overall, we observe a seasonal methane cycle (~40 ppb) with higher concentrations in winter and lower ones at the end of summer. A detailed interpretation of these variations, including a quantification of the main contributors, cannot be deduced from the atmospheric measurements alone and would require atmospheric transport modeling.

280 CO concentration in the atmosphere is much lower than that of CO_2 or CH_4. It is emitted by combustion reactions (fossil fuel and biomass burning) and is therefore used to trace emissions from human activities. In cities, it is a tracer of emissions mainly linked to road traffic and residential heating. Photochemistry (mainly active in summer), including the degradation of CO by the OH hydroxyl radical, is the main sink for carbon monoxide in the troposphere (*Badr et al.* 1995) and is responsible for its short lifetime. As a result, CO concentrations are larger in winter than in summer.

285 High concentrations of the three gases have been measured at all stations during the winter 2016/2017 (with less intensity and duration at the peri-urban stations more remote from the center of Paris, such as SAC and AND stations). The daily average concentrations reached up to 600 ppm CO_2, 2600 ppb CH_4 and 1650 ppb CO in the center of Paris, and the episode lasted for several weeks. This pollution episode was also observed with other pollutants such as PM_{10} and was documented in the study by *Foret et al.* 2022. This study showed that the exceptional duration and intensity of this pollution peak were
290 unprecedented for at least ten years and was caused by abnormal weather conditions with low wind speeds and high atmospheric stability, resulting in weak advection and vertical mixing. As dispersion was remarkably low, the concentrations during this extreme episode were mainly driven by emissions from sources located in the vicinity of the stations. This explains why the more rural stations SAC and AND show lower concentrations (respectively 95th percentiles of CO_2 concentrations are 469.68 and 457.94 ppm), while the JUS and CDS stations located in central Paris show the largest
295 concentrations (95th percentiles of CO_2 measurements are 487.02 and 490.85 ppm).
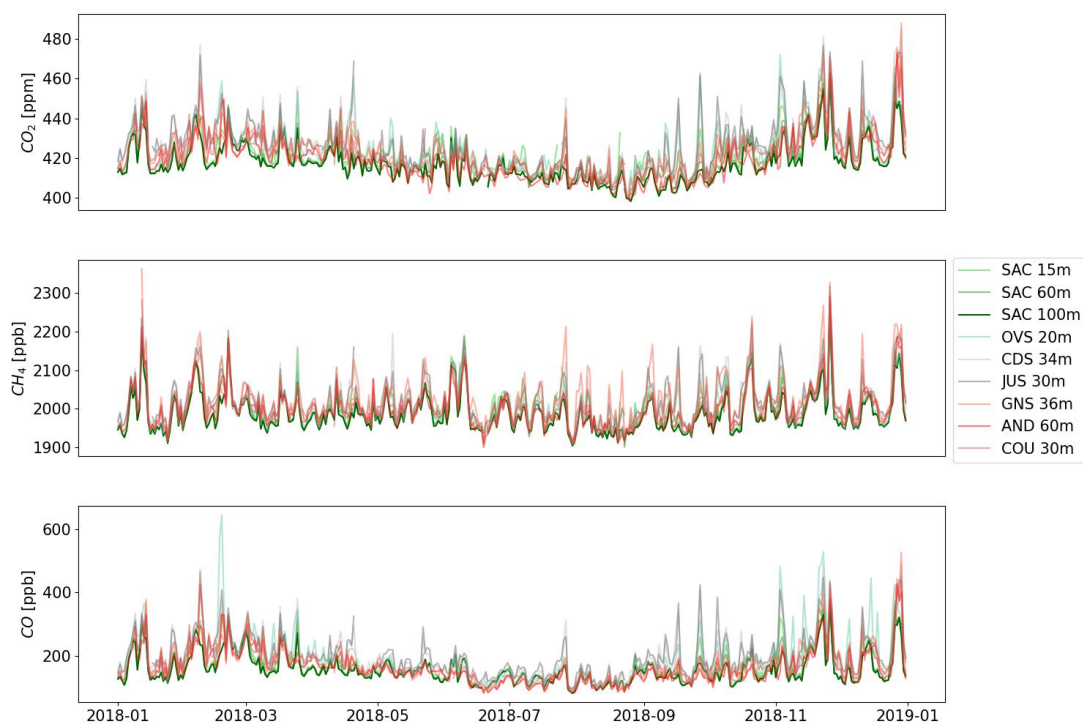
Figure 7. Parisian network daily average time series of CO_2, CH_4 and CO concentrations for the year 2018.

Fig. 7 is a focus on daily averages of CO_2, CH_4 and CO time series across the Paris' network during 2018. This year was chosen because it was the first full year in which all 7 stations were in operation with a good data availability for all of them.

300   There are three contributors to the variations in CO_2 concentration over the Paris network:

- The CO_2 emissions that are dominated by the road traffic (31%) and the residential (28%) sectors, show diurnal, weekly and seasonal cycles (c.f. AirParif's 2019 assessment of GHG emissions). In particular, 45% of the annual emissions of the residential sector occur in winter (December, January and February), compared with only 7% in summer (June, July and August), which therefore contributes to the higher CO2 concentrations during the winter

305   season in urban areas.

- Vegetation contributes to the carbon cycle in two ways: respiration, which emits CO_2, and photosynthesis, which absorbs CO_2. The two phenomena occur simultaneously at the seasonal scale (photosynthesis is only active during the day, whereas respiration contributes day and night). In spring and summer, under the effect of the sun's rays, photosynthesis is more dominant than respiration and vegetation acts as a major sink for CO_2. In winter, vegetation

310   is mostly dormant and photosynthesis is very much reduced. Vegetation and soils, via respiration, is then a source of CO_2.

- The dynamics of the boundary layer that shows large diurnal and seasonal cycles. Vertical mixing induced by convection is driven by solar heating. It is therefore absent during the night and reduced during winter with respect to summer. The atmospheric boundary layer is therefore much less developed and the vertical mixing of CO_2 is

315   weaker in winter than in summer. The CO_2 emitted is therefore more concentrated at the surface during the night
        and morning, as well as in winter (*Denning et al.* 1999).

Fig. 7 also shows CH_4 measurements. As the amplitude of the seasonal cycle is relatively small (40 ppb) with regard to the
day to day variability (~100 to 300 ppb), it is not directly perceptible in Fig. 7. In contrast to CO_2 and CO, the amplitudes of
CH_4 concentration variations appear comparable at all stations. The CH_4 concentrations and their variabilities are similar at
320 the urban stations JUS and CDS and at the peri-urban stations. The GNS station is impacted by nearby emissions although
the measurements have been filtered by the algorithm described in section 3.3. As the methane peaks observed at GNS are
mostly higher than at the other stations (0 to 1500 ppb higher), they are probably linked to local air masses that were not
detected by the wind sector filter.
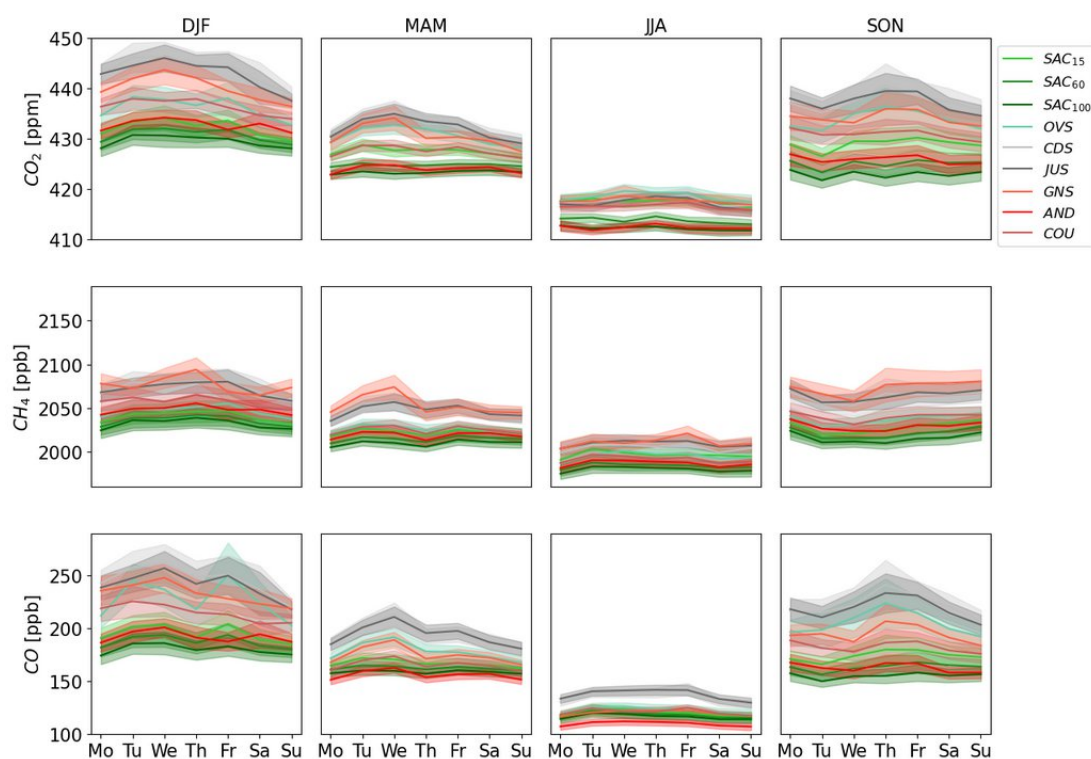
325 **Figure 8. Week cycles of CO_2, CH_4 and CO concentrations in all the stations of the Paris' network, from 2015-01-01 to 2022-12-31.**
Data are aggregated by three-month seasonal periods (DJF for winter, MAM for spring, JJA for summer and SON for autumn).

Both CO_2 and CO also show weekly variations (Fig. 8), with maximum concentrations observed on week days and minimum
on Sunday. There is no reason to believe that atmospheric dynamics or the fluxes exchanged with ecosystems have any
weekly cycle, so that anthropogenic emissions is most likely at the origin of this cycle. Higher concentrations on working
330 days and lower concentrations at weekends are expected with the variations in road traffic. According to AirParif's 2019
emission inventory, road traffic emissions during saturdays and sundays are 40% lower than those during the week. The
amplitude of the weekly cycle depends on the season and the urbanisation around the station. It varies from 1 ppm CO_2 and

5-10 ppb CO in SAC station, to 5 ppm CO_2 and 35 ppb CO in JUS station, in winter, whereas all the stations show very similar weekly cycles during the summer (1-2 ppm CO_2 and 5 ppb CO).

335   The 5% highest daily CH_4 averages at GNS station in winter (DJF) were removed before calculating the weekly cycle. This corresponds to the outliers not detected by the filters presented in section 3.3, which strongly disrupt the weekly methane cycle at this station. At all the stations, the amplitude of the CH_4 weekly cycle is fairly small and difficult to interpret. Unlike CO_2 and CO, CH_4 is not driven by local sources linked to anthropogenic activities with weekly variations such as road traffic. The main sources of CH_4 (wastes, agriculture, energy) have limited or no weekly cycles.

340   **4.2. Diurnal cycle seasonality across the Parisian network**
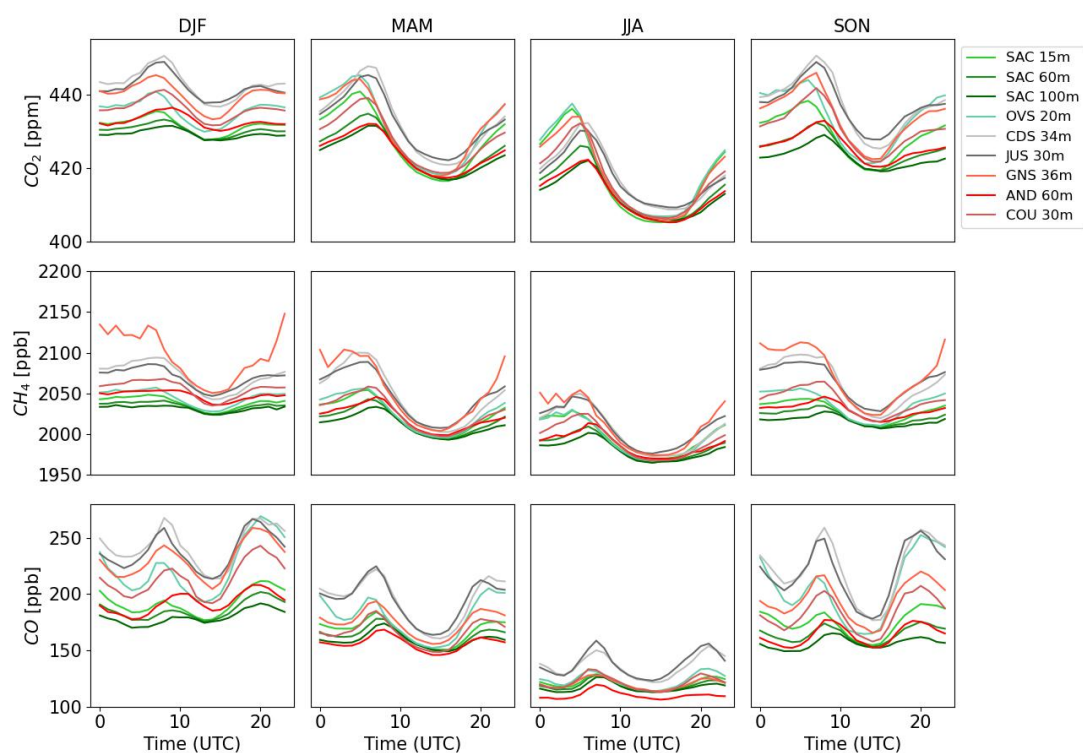
Figure 9. Diurnal cycles of CO_2, CH_4 and CO in all stations, according to the season between 2017-05-01 and 2022-12-31. Data are aggregated by three-month seasonal periods (DJF for winter, MAM for spring, JJA for summer and SON for autumn).

Fig. 9 shows the seasonally-averaged diurnal cycles at each station of the network. In order to avoid a bias due to the trend,

345   the average are calculated over a common period when all stations were in operation, between 2017-05-01 and 2022-12-31. Seasonality in the diurnal amplitude is noticeable for the three gases with larger amplitudes in summer for CO_2, while the amplitude of the diurnal cycle is maximum in winter for CO. SAC_{100} have the lowest seasonal mean concentrations across seasons and times of day, confirming the suitability of this site to provide background mixing ratios (depending on the wind direction) in forthcoming inversion studies of Paris emissions. The large amplitude in summer can be explained by the

350 largest amplitude in vertical mixing between stable nights and highly-convective afternoons combined with the high amplitude of the photosynthesis activity (only for CO_2) between day and night. The daily amplitude of biogenic activity in spring and summer are sufficiently high to play a significant role in the diurnal CO_2 cycle (*Bezyk et al.* 2021). The long-term time series and the consistency of the diurnal and seasonal cycles across the network confirm the potential of the network to investigate Paris emissions at urban to sub-regional spatial scales. Compared to CO_2, amplitudes in CH_4 diurnal cycles

355 remain fairly stable across seasons and is likely driven by vertical mixing rather than emissions. We also observe smaller gradients (less dispersed lines) across stations during daytime in the summer for all three species, another evidence of the strong vertical mixing and deeper mixing heights during the warm season. The non-typical behavior observed for CH_4 in GNS (especially at night in winter and autumn, when the vertical mixing is the weakest) suggest that the filter implemented in the data processing and presented in section 3.3 is not sufficient to filter out all the measurements that are significantly

360 affected by local sources. This should be taken into account when using the data for atmospheric inversions. We discuss later the source of the peaks by exploring peak magnitudes as a function of wind direction (cf. section 5.1). In comparison, CO mixing ratios' seasonality is fairly constant, slightly larger in winter than summer, contrary to the ones of CO_2 and CH_4. According to AirParif's emissions inventory for 2019, CO emissions in the Île-de-France region are mainly driven by emissions from residential heating (48.5%). However, these emissions occur mainly in winter and are relatively constant

365 over the course of a day. The second largest source of CO emissions is road traffic (28.5%). These emissions, on the other hand, vary widely throughout the day (peaking at road traffic peak times in the morning and evening, and falling to a minimum at night). It is therefore this sector of emissions combined with the dynamics of the boundary layer that seems to drive the daily cycle of carbon monoxide concentrations in the Paris region.

5. Gradients between pairs of stations

370 Measurements of CO_2, CH_4 and CO acquired at SAC_{100} station are almost always the lowest and with the smallest variations among the stations in the Paris network. This is because SAC station is a relatively isolated station, located in a fairly vegetated and low urbanized area. When the weather is very stable (especially at night and during winter), the top of the ICOS tall tower is located above the atmospheric boundary layer. In this case, the measurements at SAC_{100} station are not representative of the local surface emissions. Measurements at this station will therefore be considered as "background

375 measurements" in this section except when the wind is coming from the North (12% of the time). In the present section, we will look at the gradients between the Paris network measurements and the SAC_{100} station measurements for the three species. The gradients are denoted Δ.

The concentration gradients between pairs of stations are the signal interpreted by atmospheric inversions to quantify the regional fossil CO_2 emissions and biogenic CO_2 sources and sinks int the Paris area (*Breon et al.* 2015; *Stauffer et al.* 2016;

380 *Lian et al.* 2023). In those studies, the gradients are usually selected for daytime because during the night, in the absence of vertical mixing, the measured concentration is very much a function of the altitude and model-measurements comparisons

are difficult. Work is underway to develop the assimilation of night-time data so, in the rest of this section, we will use the gradients measured over the whole day.

Wind speed and direction are acquired at SAC_{100} station (a relatively isolated station with measurements taken high above ground level). In the following, the wind speed measured at the top of the SAC station's tall tower is considered representative of the regional wind.

5.1. Annual gradients upwind and downwind conditions between each station and SAC_{100}
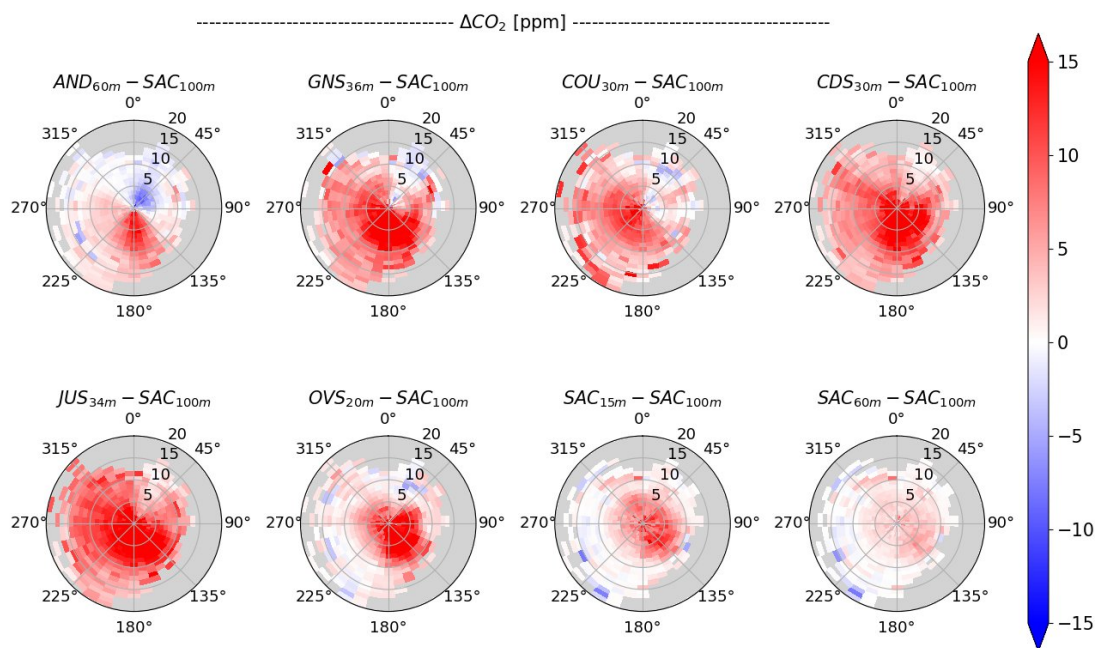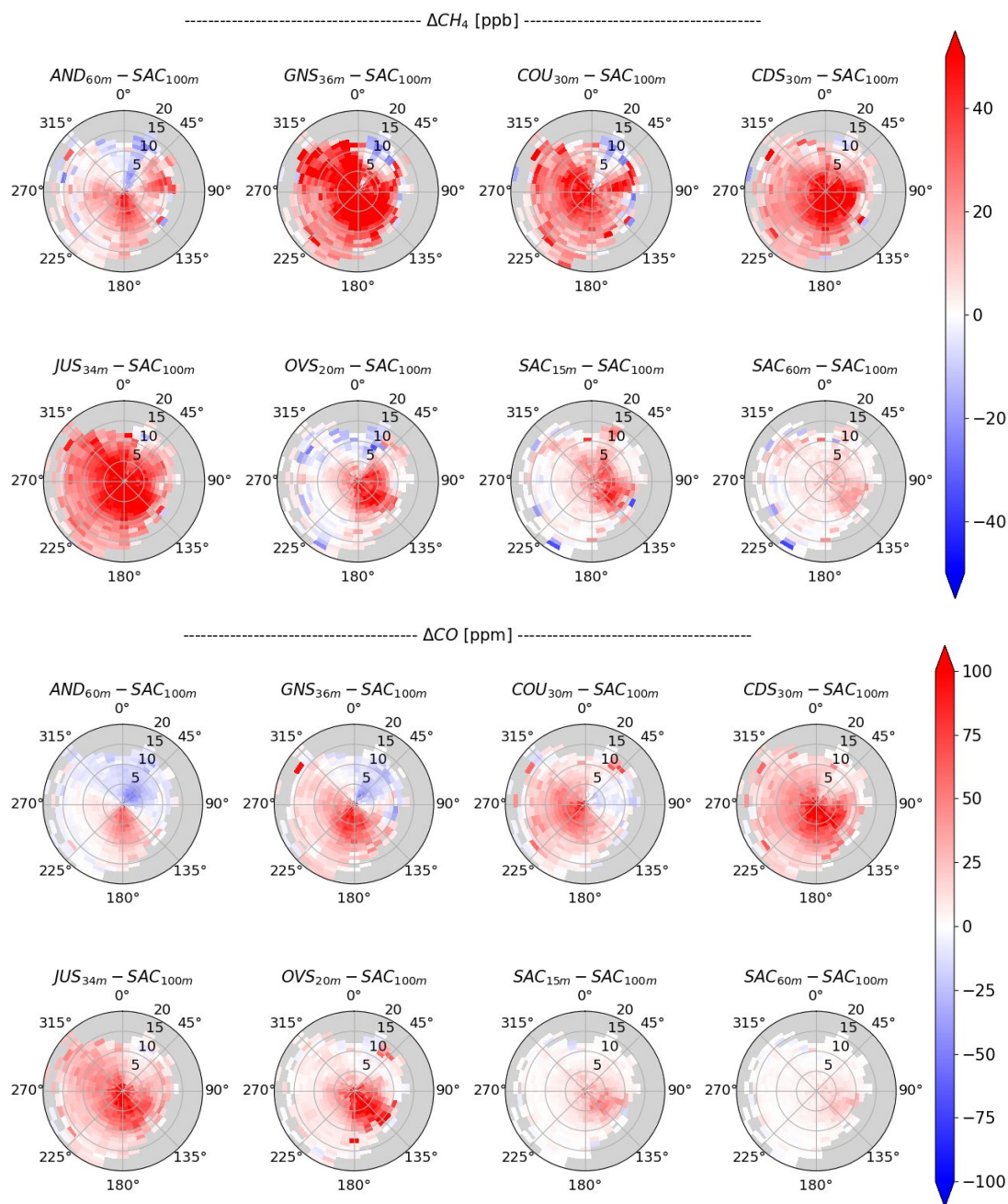
390

Figure 10. Representation of the CO₂, CH₄ and CO molar fraction differences between one given site from the Parisian network and measurements from SAC₁₀₀ depending on wind speed (radius) and wind direction (angle). All the measurements are binned in 1 m.s⁻¹ and 10° sectors. Hourly average from 2015-01-01 to 2022-12-31, depending on the data availability from each measurement site (see table 1).

395   Fig. 10A (upper part) shows the mean gradients of CO_2 (ΔCO_2) between a station and SAC_{100} used as a reference, as a function of wind speed and direction. Generally, peri-urban stations when located downwind of SAC station (S and SW wind direction) show positive ΔCO_2 values reflecting net emissions from the city, and when located upwind of SAC station, they show negative values. Between the tall towers of AND and SAC where measurements are conducted at 100 meters above ground level, ΔCO_2 values are between 14 and 20 ppm when the wind is from SW and between -10 and -20 ppm when the

400   wind is from the NE, thus a rather symmetrical distribution of ΔCO_2 values with wind direction. Between the stations north of Paris COU and GNS where measurements are performed at $\approx$ 30 m above the ground, and SAC station, there are more positive ΔCO_2 values for a larger range of wind directions. The positive values of ΔCO_2 at GNS station (between 10 and 15 ppm) are higher than at COU station (between 5 and 10 ppm) under SW winds direction, indicating that the GNS station lies in the center of the Paris plume when the wind is more or less aligned with the SAC-GNS direction, while COU station is

405   more on the side of the plume. Between the two urban stations located in the center of Paris CDS and JUS stations, the distribution of ΔCO_2 as a function of wind direction is similar, with positive values (about 15 ppm CO2 or more) from all sectors and higher values when the wind is from the S at CDS station, that is, this station receiving CO_2 from emissions in the southern part of the city. When the wind is from the N at CDS or JUS stations, one would expect SAC station to be higher in CO_2, that is a negative ΔCO_2 value in the figure. This is not the case, probably because of the influence of high

410   emissions in the vicinity of CDS that impact this station measurements permanently. Between the two southern stations SAC and OVS both located in the South-West of Paris, there are positive ΔCO_2 values when the wind is from the SE (OVS is then downwind from SAC). However, as the two stations are geographically close but with different sampling heights, the OVS-SAC gradient in a SE wind does not fully reflect emissions from the area between the two stations. In order to obtain more representative information, we need to take into account the vertical gradient between the height of the air sample at the OVS

415   station (20 m a.g.l) and the height of the sample at SAC station (100 m a.g.l). To do this, we can observe the gradient between SAC_{15} and SAC_{100} stations, which is approximately 5 ppm CO_2. It thus seems that the spatial gradient between OVS and SAC_{100} stations is the result of both emissions between the two sites and differences in altitude collection.

The ΔCO gradients of all stations with respect to SAC displayed in Fig. 10 are broadly similar to the ΔCO_2 ones, but with more contrasted positive and negative sectors, meaning that the background 'clean air' value of CO in the NE sector at AND

420   station, in the E sector at COU station and in the NE sector at GNS station is relatively lower than the one of CO_2. This may be due to low traffic emissions causing low CO concentrations in the upwind source area of AND, COU and GNS stations. For the two urban stations CDS and JUS, ΔCO values are positive for all wind sectors and, just like for ΔCO_2, they are significantly higher (~ 60 ppb) when the wind is from the SW to the SE sector, consistent with dominant traffic emissions increasing both ΔCO and ΔCO_2 inside the city compared to SAC station.

425   The ΔCH_4 distribution shown in Fig. 10 is broadly similar to that of ΔCO_2 as a function of wind direction and wind speed, but high ΔCH_4 values for high wind speeds compared to low wind speeds in the E sector at AND station, and in the NW and E sectors at COU station suggest remote CH_4 sources influencing these two sites. The most striking difference of ΔCH_4 with respect to ΔCO_2 and ΔCO is observed at GNS station which has very high ΔCH_4 for all sectors, in particular from the NW

and for low wind speeds. This specific signature suggests the existence of a large source of CH_4 in the immediate vicinity of
430 GNS station, most likely the landfill located 2.5 km from GNS station in the N - NNW direction, but also from other sources
such as leaks in the gas transmission network. This pollution source is still visible, even if the data are filtered with the
statistical and wind sector filters implemented in the data processing.

In all cases, strong gradients are observed when the wind is weak and weak gradients when the wind is strong (Fig. S1). This
reflects the phenomenon of ventilation. When the wind is weak, the emissions accumulate in the slow air mass and create
435 strong gradients with the background (> 15 ppm CO_2 at JUS). Strong winds cause emissions to be ventilated and diluted in
the air stream (~ 3 to 5 ppm CO_2 at JUS for a 15 m/s wind speed).

5.2. Seasonal gradients between each station and background (SAC_{100})
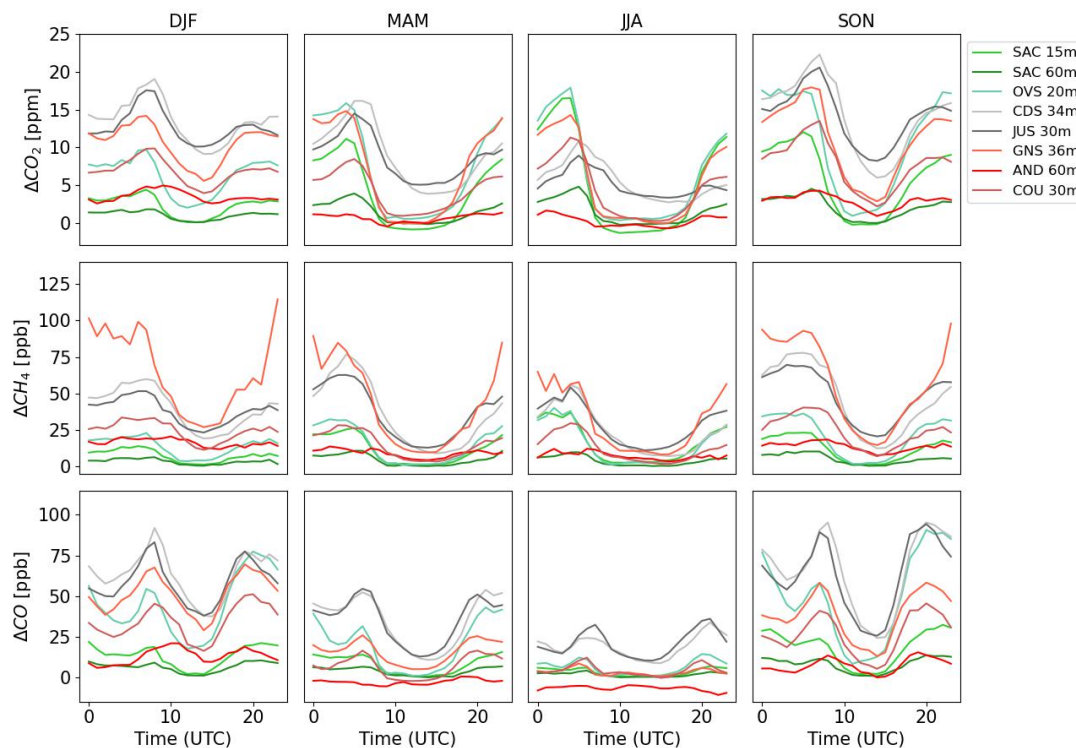
Figure 11. Diurnal cycles of ΔCO₂, ΔCH₄ and ΔCO gradients in all stations, according to each season between 2017-05-01 and
440 **2022-12-31.**

The seasonal distribution of ΔCO_2 given in Fig. 11 indicates more pronounced ΔCO_2 between upwind stations and SAC_{100}
station during the winter and the autumn seasons, and smaller contrasts in spring and summer. The fact that ΔCO_2 is more
contrasted in autumn and winter than during the growing season is partly explained by the diurnal covariance (or diurnal
vegetation rectification first found by *Denning et al.* 1995) of vegetation fluxes with vertical mixing. In the growing season,
445 higher CO_2 uptake by the vegetation in the day occurs at the same time with a higher CO_2 emission by plant and soil

respiration in the night, and the covariance between daytime uptake with strong vertical mixing and nighttime release by the vegetation with suppressed mixing should induce a more positive average ΔCO_2 gradient in all sectors in spring and summer than in the other seasons, as observed in Fig. 11.

The two urban stations CDS and JUS stations always have the largest enhancements of CO_2 and CO compared to SAC
450 station, those positive gradients being larger in winter (10-20 ppm), which illustrates the strong signal of the emissions from the Paris area compared to background seasonal changes. In summer, CDS and JUS stations keep a positive ΔCO_2 gradient with respect to SAC station (see also Fig. 11), but this gradient is of smaller amplitude (5-10 ppm) than in winter, mainly from stronger vertical mixing and lower emissions (especially emissions related to heating). The OVS station located at the same distance than SAC station from the main city emissions still has higher values of CO and CO_2 than SAC station all year
455 round. This may be explained by urban emissions in the footprint of this station, but also by the altitude above ground level of the sampling line which is much lower in OVS station (20m) than in SAC station (100m).

6. Co-variability of CO_2 or CH_4 and CO concentrations, link with drivers of CO_2 and CH_4 concentrations

In the following, we analyze how the concentration of the three gases CO_2, CH_4 and CO co-vary in time. For such analysis, it is necessary to substract the trend and seasonal cycle in the concentration time series. We use the time series of the gases,
460 compute a 3 month rolling average and derive a residual as the difference between the measurement and the temporal average. In the following, we analyze these residuals co-variations.

6.1. Co-variability of CO2 and CO
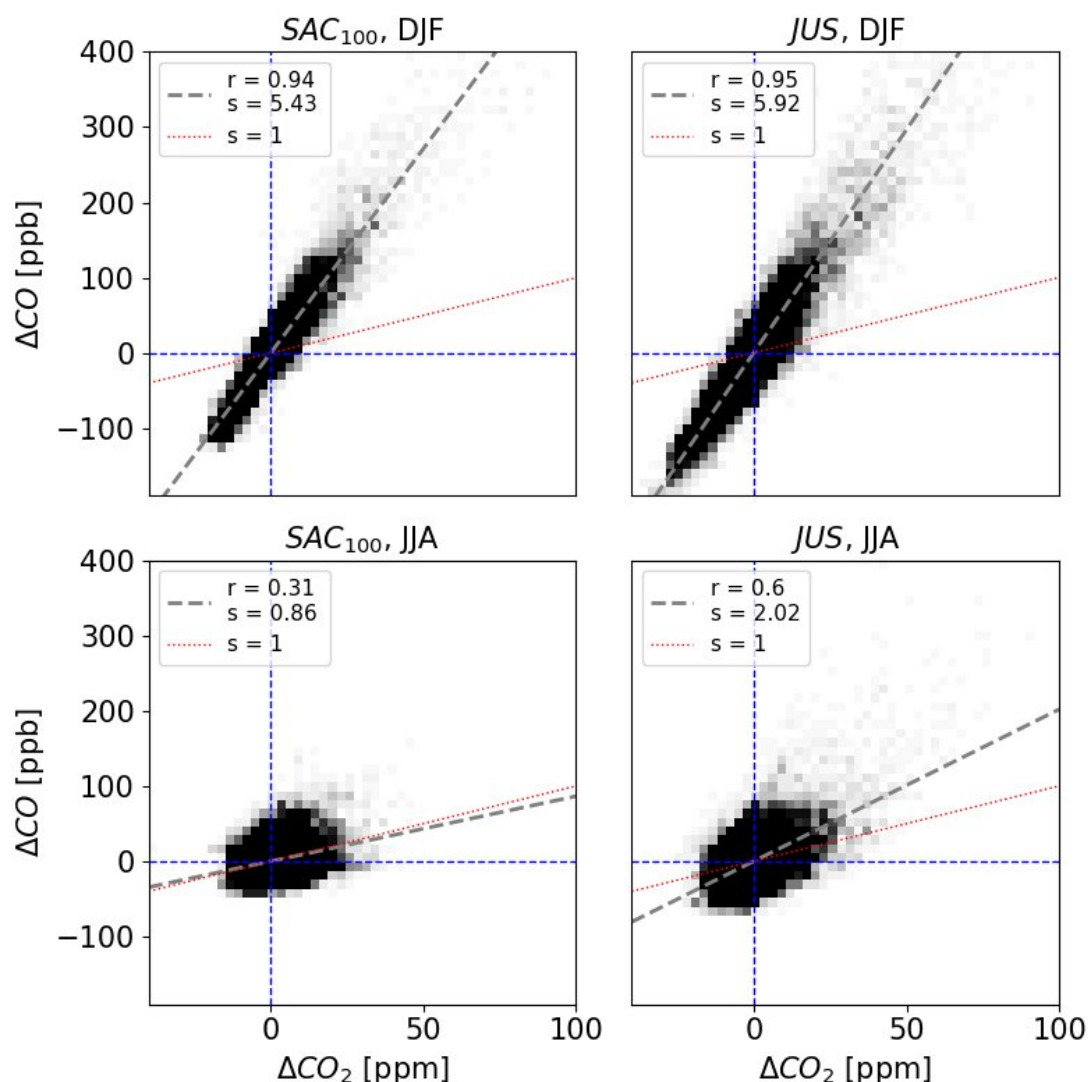
**Figure 12. Histogram of the co-variability of CO_2 and CO detrended measurements (i.e. differences between daily measurements
465 and 3 months rolling average), in JUS and SAC_{100} station, from 2015-01-01 to 2022-12-31 according to the season (summer [JJA]
and winter [DJF]). The grey doted lines are representing the linear regressions.**

CO (carbon monoxide) is a gas emitted by imperfect combustion (fossil fuels, vegetation fires, etc.) that also emit CO_2. Its
lifespan of a few weeks or months is much shorter than that of CO_2 (around a hundred years) and CH_4 (around a decade). It
therefore does not accumulate in the atmosphere, which makes it, in urban areas, a good indicator of emissions linked to
470 anthropogenic activities such as road and air traffic or residential heating (wood and gas in Paris). These sources have very
different CO/CO_2 emission ratios depending on their nature. According to the latest AirParif inventory (2019), the residential

sector has a CO/CO_2 ratio of around 1.84 [T/kT] (i.e. 2.89 mmol.mol^{-1}), while road traffic has a ratio closer to 3.44 [T/kT] (i.e. 5.41 mmol.mol^{-1}).

Fig. 12 is a histogram of the co-variabilities of CO and CO_2 between 2015 and 2022, in winter (DJF) and summer (JJA), in
475 the SAC_{100} (rural) and JUS (urban) stations. These were chosen because they are representative of the overall behaviour of measurements at all the stations in the Paris network. The linear regressions are represented by the dotted lines. The correlation coefficients and slopes of the regression lines are also shown. In winter, there is a strong co-variation between the two species due to day-to-day variations (diurnal cycle would have the same impact on summer), with high correlation coefficients. The strongest correlations are observed in the center of Paris, at JUS and CDS stations with a correlation
480 coefficient r=0.96. The lowest correlation coefficient is observed at the OVS station with r=0.87, which remains rather high. This may be due to the local sources mentioned in section 3.3. The other stations (SAC, AND, COU, GNS stations) all have correlation coefficients of 0.92>=r>=0.94. This reflects the fact that CO_2 emissions are mainly driven by human activities in winter. This is mainly the case in the center of Paris, but also in more rural stations such as SAC station.

In summer, correlations are much weaker at all stations. The highest correlation coefficients are always observed at stations
485 in the center of Paris, with r_{JUS}=0.57 and r_{CDS}=0.61. The OVS station still has a high correlation coefficient (r=0.51) compared with the other stations outside Paris (0.26>=r>=0.41) due to the local sources of pollution identified earlier. The correlation coefficients for SAC_{15} (0.34), SAC_{60} (0.31) and SAC_{100} (0.26) are lower than those for COU (0.41), AND (0.33) and GNS (0.38) stations.This reflects the fact that CO_2 concentrations are mainly driven by biogenic activity in summer. This has a significant influence on CO_2, even in the center of Paris.

6.2. Co-variability of CH$_4$ and CO
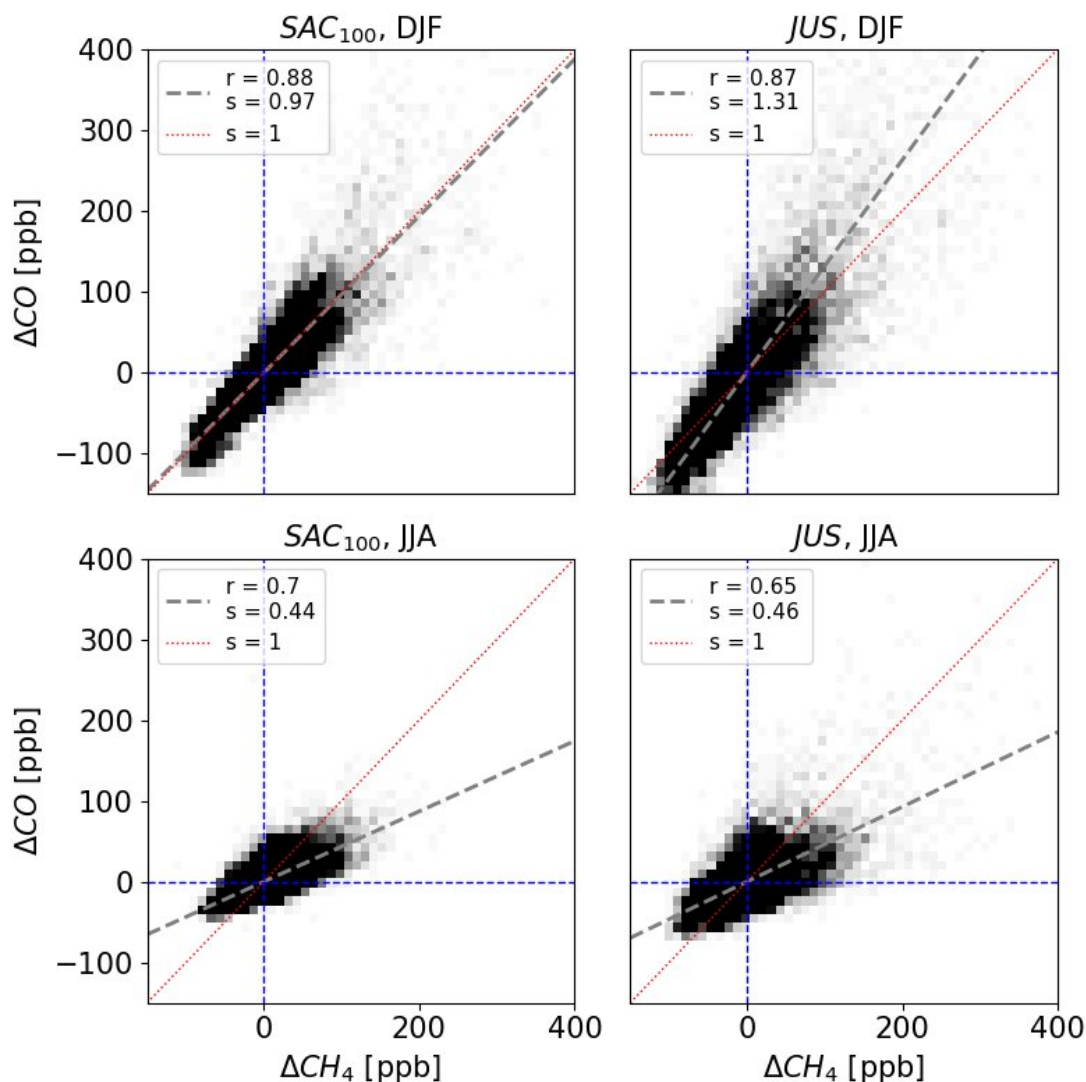
Figure 13. Histogram of the co-variability of CH$_4$ and CO detrended measurements (i.e. differences between daily measurements and 3 months rolling average), in SAC$_{100}$ and JUS stations, from 2015-01-01 to 2022-12-31 according to the season (summer [JJA] and winter [DJF]). The doted lines are representing the linear regressions.

Methane is mainly emitted by leaks in urban gas distribution networks and by anaerobic methanogenic bacteria in wetlands. In these two cases, there is no co-emission of CO. Bio-fuels may be responsible for co-emission of CO and CH$_4$, but this remains a minority.

In winter, there is a fairly strong correlation between CH$_4$ and CO at all the stations in the Paris network (see Fig. 13). The measurements from the OVS and GNS stations are affected by the local pollution described in sections 3.3. The other stations in the network have correlations of between 0.82 (COU) and 0.89 (SAC). The highest correlation is at SAC station,

which is close to a natural wetland area. In summer, the correlations are greater than for CO_2. The correlation coefficient remains high at SAC station (r=0.7), whereas it falls much further at the other stations in the network (down to 0.42 at GNS). This reflects the smaller amplitude of the seasonal methane cycle compared with that of CO_2.

505 As methane sources are different from CO sources, it was not expected to find such a strong correlation between these two species. We assume that the sources of methane and carbon monoxide are colocated in the footprint of the stations, but that they are not identical. The correlation between these two species is due to the colocation of these sources and to the dynamics of the amosphere that affects all the air mass. In order to investigate this possibility, we will study the emission maps for these two species and determine the extent to which the sources of CO and CH_4 coincide (or not) in a future work.

7. Conclusion and perspectives

510 With a population of 12 million inhabitants, 37 Mt CO_2eq emitted in 2021 and being relatively isolated from other major urban areas, the Paris region is well suited to analyse the link between a city's CO_2 emissions and the resulting variations in atmospheric concentrations. Seven stations were installed in Paris and its surounding areas between 2014 and 2017. Each of them is equipped with a Cavity Ring-Down Spectrometer (CRDS) enabling measurements of atmospheric concentrations of carbon dioxide (CO_2), methane (CH_4) and carbon monoxide (CO). A great deal of work has gone into guaranteeing the

515 quality of the data by carrying out regular maintenances, biannual calibrations, daily target gas injections and data quality control. Measurements are automatically sent to a dedicated database and made available in near-real time (NRT). High-frequency variations in CO_2, CH_4 and CO measurements are automatically filtered by a statistical algorithm. Larger perturbations are observed for GNS and OVS stations due to well-defined local sources. For this reason, an additional filter using wind speed and direction has been implemented to filter out these residual disturbances.

520 Long-term continuous measurements allow us to observe a seasonal cycle that is consistent between stations, with an amplitude of around 20 ppm CO_2, a maximum at the end of winter and a minimum at the end of summer. The increase trend of 2.34 ppm CO_2/year is consistent with the increase measured at background stations such as Mauna Loa (Hawaii, USA). As CO is emitted by combustions, the decrease trend of -3 ppb CO/year highlights the higher and higher efficiency of residential heaters and internal combustion engines.

525 The seasonal, weekly and daily cycles of CO_2, CH_4 and CO are mainly driven by several factors:

- Photosynthesis absorbs CO_2 (only) from the atmosphere when activated by sunlight. This is why photosynthesis is very active in spring and summer, and makes a major contribution to reducing CO_2 concentrations in the atmosphere during this period. In winter, there is little or no photosynthesis. Respiration therefore dominates the biogenic activity and increases the CO_2 concentrations measured in all stations. Conversely, methane and carbon
530 monoxide are not affected by biogenic activity.

- The dynamics of the atmospheric boundary layer impacts the daily cycle of concentrations. Atmospheric convection is driven by solar heating and dilutes the gases that have been accmulating near the surface during the night. This

process is more efficient during the summer than in winter and impacts all gases. However, the impact of this effect is most visible on the methane daily cycle, as it is neither affected by variations in emissions nor by biogenic activity.The methane concentration at all stations decreases in the morning and increases in the evening. The amplitude of this cycle is around 25 ppb and is consistent between all the stations. The dynamics of the atmospheric boundary layer also affect the seasonal cycle of species. In winter, concentrations are larger due to the weak development of the boundary layer, even during the day. In summer, on the other hand, the boundary layer is more developed, which contributes to the minimum of the seasonal cycle for all species.

- Anthropogenic emissions of CO_2 and CO, which are high in winter (mainly due to residential heating) and lower in summer, explain part of the seasonal cycle. They are also responsible for the weekly cycle, as road traffic is much more intense during the week (Monday to Friday) than at weekends (Saturday and Sunday). The peaks in CO_2 and CO observed in the morning and evening in the daily cycle are also explained by emissions linked to the peak hours of road traffic. Unlike CO_2 and CO, methane emissions do not show a significant cycle, which is expected as their main sources are waste, leaks in the city gas transport network and agricultures.

The very strong correlation between the measurements of carbon monoxide and carbon dioxide concentrations (without the seasonal cycle of these two species in order to concentrate as much as possible on exchanges with the surface) confirm that CO_2 concentrations variations are mainly driven by anthropogenic emissions in winter at all the stations (r = 0.94 at SAC and r = 0.95 at JUS). In summer, the biogenic sink has a strong impact so that the variability of CO2 is driven by other factors which reduces the correlation between CO and CO2 variations (r = 0.31). Within the city centre, the contribution of anthropogenic emissions remains higher than outside of Paris, so that the CO-CO2 correlations remains high in summer (r = 0.6).

The gradients calculated between the measurements taken at the stations and SAC_{100} (background for the prevailing wind) are the information assimilated by the inversion systems for calculating emissions. For each station, the gradient calculated is representative of the surface emissions between that location and SAC for the corresponding wind direction, diluted in the moving air mass. Stations located in predominantly urban areas (JUS, CDS) show systematically positive gradients (90th percentiles in both stations: ~30 ppm CO_2, ~95 ppb CH_4, ~135 ppb CO in winter and ~12 ppm CO_2, ~60 ppb CH_4, ~50 ppb CO in summer), with no dependence on wind direction. In contrast, AND station (in a much less urbanised area) shows a strong variation of the gradient with respect to wind direction. Gradients should only be used to calculate emissions after careful selection of the data. A deviation from the wind direction implies that the plume observed with the downwind station changes. For example, when the wind is on the SAC-GNS axis, the GNS station is located in the plume of the center of Paris, whereas the COU station is located in the plume of the suburbs and therefore shows a weaker signal.

The study of CO_2, CH_4 and CO concentration measurements has enabled us to identify systematic temporal variations due to boundary layer dynamics, biogenic activity and variations in anthropogenic emissions. It remains necessary to use an atmospheric transport model coupled to a land surface (vegetation activity) surface model to attribute more precisely the

contributions of each component to the measurements presented in this study. The use of such a model is one of the possible applications of the data available by the scientific community.

Competing interests

The contact author has declared that none of the authors has any competing interests.

570 **Acknowledgements**

The authors have received funding from the Pilot Applications in Urban Landscapes – Towards integrated city observatories for greenhouse gases (PAUL) project, from the European Union's Horizon 2020 research and innovation program under grant agreement no. 101037319 (ICOS-Cities).

The authors would like to acknoledge the QUALAIR team and infrastructure for their scientific support. QUALAIR is an

575 observation plateform of the OSU EcceTerra of Sorbonne University operated by LATMOS with the support of IPSL.

References

[1] World bank based on date from un population division – processed dby our world in data. "urban population" [dataset]. World bank based on data fraom the un population division [original data].

[2] A. Agustí-Panareda, S. Massart, F. Chevallier, S. Boussetta, G. Balsamo, A. Beljaars, P. Ciais, N. M. Deutscher, R.

580 Engelen, L. Jones, R. Kivi, J.-D. Paris, V.-H. Peuch, V. Sherlock, A. T. Vermeulen, P. O. Wennberg, and D. Wunch, Forecasting global atmospheric CO_2, Atmospheric Chemistry and Physics, 14 (2014), pp. 11959–11983.

[3] Émissions de polluants atmosphériques et de gaz à effet de serre, bilan Île-de-france, année 2019, tech. rep., AirParif, 10 2022.

[4] Inventaire air-climat-Énergie, bilan Île-de-france, année 2021, tech. rep., Air Parif, 03 2024.

585 [5] I. Albarus, G. Fleischmann, P. Aigner, P. Ciais, H. Denier van der Gon, R. Droge, J. Lian, M. A. Narvaez Rincon, H. Utard, and T. Lauvaux, From political pledges to quantitative mapping of climate mitigation plans : Comparison of two European cities, Carbon Balance and Management, 18 (2023), p. 18.

[6] O. Badr and S. Probert, Sinks and environmental impacts for atmospheric carbon monoxide, Applied Energy, 50 (1995), pp. 339–372.

590 [7] Y. Bezyk, I. Sówka, and M. Górka, Assessment of urban CO2 budget : Anthropogenic and biogenic inputs, Urban Climate, 39 (2021), p. 100949.

[8] X. Bonnemaizon, P. Ciais, C. Zhou, S. B. Arous, S. J. Davis, and N. Megel, Scaling traffic variables from sensors sample to the entire city at high spatiotemporal resolution with machine learning: Applications to the Paris megacity, Environmental Research : Infrastructure and Sustainability, 4 (2024), p. 035010.

[9] H. Braud, R. Sarda-Estève, P. Bousquet, M. Ramonet, R. Sarda, and P. Ciais, CO/CO$_2$ ratio in urban atmosphere : Example of the agglomeration of Paris, France.

[10] F. M. Bréon, G. Broquet, V. Puygrenier, F. Chevallier, I. Xueref-Remy, M. Ramonet, E. Dieudonné, M. Lopez, M. Schmidt, O. Perrussel, and P. Ciais, An attempt at estimating Paris area CO$_2$ emissions from atmospheric concentration measurements, Atmospheric Chemistry and Physics, 15 (2015), pp. 1707–1724.

[11] A. Christen, L. Emmenegger, S. Hammer, W. Kutsch, C. D'Onofrio, J. Chen, M. Eritt, M. Haeffelin, L. Järvi, N. Kljun, T. Lauvaux, B. Loubet, M. Mauder, A. A. Mensah, D. Papale, L. Rivier, S. Stagakis, and A. Vermeulen, ICOS pilot observatories to monitor greenhouse gas emissions from three different-size european cities, Copernicus GmbH, 2023.

[12] P. Cristofanelli, C. Fratticioli, L. Hazan, M. Chariot, C. Couret, O. Gazetas, D. Kubistin, A. Laitinen, A. Leskinen, T. Laurila, M. Lindauer, G. Manca, M. Ramonet, P. Trisolino, and M. Steinbacher, Identification of spikes in continuous ground-based in situ time series of CO 2 , CH 4 and CO: An extended experiment within the European ICOS Atmosphere network, Atmospheric Measurement Techniques, 16 (2023), pp. 5977–5994.

[13] Plan climat de paris, vers une ville neutre en carbone, 100% énergies renouvelables, résiliente, juste et inclusive, tech. rep., Ville de Paris, 2018.

[14] S. M. Defratyka, J.-D. Paris, C. Yver-Kwok, J. M. Fernandez, P. Korben, and P. Bousquet, Mapping Urban Methane Sources in Paris, France, Environmental Science & Technology, 55 (2021), pp. 8583–8591.

[15] A. S. Denning, I. Y. Fung, and D. Randall, Latitudinal gradient of atmospheric CO2 due to seasonal exchange with land biota, Nature, 376 (1995), pp. 240–243.

[16] A. S. Denning, M. Holzer, K. R. Gurney, M. Heimann, R. M. Law, P. J. Rayner, I. Y. Fung, S.-M. Fan, S. Taguchi, P. Friedlingstein, Y. Balkanski, J. Taylor, M. Maiss, and I. Levin, Three-dimensional transport and concentration of SF$_6$: A model intercomparison study (TransCom 2), Tellus B : Chemical and Physical Meteorology, 51 (1999), p. 266.

[17] F. Dietrich, J. Chen, B. Voggenreiter, P. Aigner, N. Nachtigall, and B. Reger, MUCCnet : Munich Urban Carbon Column network, Atmospheric Measurement Techniques, 14 (2021), pp. 1111–1126.

[18] G. Foret, V. Michoud, S. Kotthaus, J.-E. Petit, A. Baudic, G. Siour, Y. Kim, J.-F. Doussin, J.-C. Dupont, P. Formenti, C. Gaimoz, V. Ghersi, A. Gratien, V. Gros, J.-L. Jaffrezo, M. Haeffelin, M. Kreitz, F. Ravetta, K. Sartelet, L. Simon, Y. Té, G. Uzu, S. Zhang, O. Favez, and M. Beekmann, The December 2016 extreme weather and particulate matter pollution episode in the Paris region (France), Atmospheric Environment, 291 (2022), p. 119386.

[19] B. D. Hall, A. M. Crotwell, D. R. Kitzis, T. Mefford, B. R. Miller, M. F. Schibig, and P. P. Tans, Revision of the World Meteorological Organization Global Atmosphere Watch (WMO/GAW) CO$_2$ calibration scale, Atmospheric Measurement Techniques, 14 (2021), pp. 3015–3032.

625   [20] J. Heiskanen, C. Brümmer, N. Buchmann, C. Calfapietra, H. Chen, B. Gielen, T. Gkritzalis, S. Hammer, S. Hartman, M. Herbst, I. A. Janssens, A. Jordan, E. Juurola, U. Karstens, V. Kasurinen, B. Kruijt, H. Lankreijer, I. Levin, M.-L. Linderson, D. Loustau, L. Merbold, C. L. Myhre, D. Papale, M. Pavelka, K. Pilegaard, M. Ramonet, C. Rebmann, J. Rinne, L. Rivier, E. Saltikoff, R. Sanders, M. Steinbacher, T. Steinhoff, A. Watson, A. T. Vermeulen, T. Vesala, G. Vítková, and W. Kutsch, The Integrated Carbon Observation System in Europe, Bulletin of the American Meteorological Society, 103 (2022), pp.
630   E855–E872.

[21] E. González del Castillo, N. Taquet, A. Bezanilla, W. Stremme, M. Ramonet, O. Laurent, Y. Xu, M. Delmotte, CO_2 variability in the Mexico City region from in situ measurements at an urban and a background site, Atmósfera, 35 (2022), pp. 377–393.

[22] Intergovernmental Panel on Climate Change (IPCC), Climate Change 2022 – Impacts, Adaptation and Vulnerability:
635   Working Group II Contribution to the Sixth Assessment Report of the Intergovernmental Panel on Climate Change, Cambridge University Press, 1 ed., June 2023.

[23] T. Lauvaux, K. R. Gurney, N. L. Miles, K. J. Davis, S. J. Richardson, A. Deng, B. J. Nathan, T. Oda, J. A. Wang, L. Hutyra, and J. Turnbull, Policy-Relevant Assessment of Urban CO_2 Emissions, Environmental Science & Technology, 54 (2020), pp. 10237–10245.

640   [24] J. Lian, F.-M. Bréon, G. Broquet, T. Lauvaux, B. Zheng, M. Ramonet, I. Xueref-Remy, S. Kotthaus, M. Haeffelin, and P. Ciais, Sensitivity to the sources of uncertainties in the modeling of atmospheric CO_2 concentration within and in the vicinity of Paris, Atmospheric Chemistry and Physics, 21 (2021), pp. 10707–10726.

[25] J. Lian, O. Laurent, M. Chariot, L. Lienhardt, M. Ramonet, H. Utard, T. Lauvaux, F.-M. Bréon, G. Broquet, K. Cucchi, L. Millair, and P. Ciais, Development and deployment of a mid-cost CO_2 sensor monitoring network to support atmospheric
645   inverse modeling for quantifying urban CO_2 emissions in Paris, Jan. 2024.

[26] J. Lian, T. Lauvaux, H. Utard, F.-M. Bréon, G. Broquet, M. Ramonet, O. Laurent, I. Albarus, M. Chariot, S. Kotthaus, M. Haeffelin, O. Sanchez, O. Perrussel, H. A. Denier van der Gon, S. N. C. Dellaert, and P. Ciais, Can we use atmospheric CO_2 measurements to verify emission trends reported by cities ? Lessons from a 6-year atmospheric inversion over Paris, Atmospheric Chemistry and Physics, 23 (2023), pp. 8823–8835.

650   [27] J. Lian, T. Lauvaux, H. Utard, F.-M. Bréon, G. Broquet, M. Ramonet, O. Laurent, I. Albarus, K. Cucchi, and P. Ciais, Assessing the Effectiveness of an Urban CO_2 Monitoring Network over the Paris Region through the COVID-19 Lockdown Natural Experiment, Environmental Science & Technology, 56 (2022), pp. 2153–2162.

[28] Z. Liu, C. He, Y. Zhou, and J. Wu, How much of the world's land has been urbanized, really ? A hierarchical framework for avoiding confusion, Landscape Ecology, 29 (2014), pp. 763–771.

655   [29] V. Mahajan, G. Cantelmo, R. Rothfeld, and C. Antoniou, Predicting network flows from speeds using open data and transfer learning, IET Intelligent Transport Systems, 17 (2023), pp. 804–824.

[30] P. Martino, Atlas of the Human Planet 2016. Mapping Human Presence on Earth with the Global Human Settlement Layer.

[31] L. Menut, B. Bessagnet, G. Siour, S. Mailler, R. Pennel, and A. Cholakian, Impact of lockdown measures to combat
660   Covid-19 on air quality over western Europe, Science of The Total Environment, 741 (2020), p. 140426.

[32] L. E. Mitchell, J. C. Lin, L. R. Hutyra, D. R. Bowling, R. C. Cohen, K. J. Davis, E. DiGangi, R. M. Duren, J. R.
Ehleringer, C. Fain, M. Falk, A. Guha, A. Karion, R. F. Keeling, J. Kim, N. L. Miles, C. E. Miller, S. Newman, D. E. Pataki,
S. Prinzivalli, X. Ren, A. Rice, S. J. Richardson, M. Sargent, B. B. Stephens, J. C. Turnbull, K. R. Verhulst, F. Vogel, R. F.
Weiss, J. Whetstone, and S. C. Wofsy, A multi-city urban atmospheric greenhouse gas measurement data synthesis,
665   Scientific Data, 9 (2022), p. 361.

[33] , A multi-city urban atmospheric greenhouse gas measurement data synthesis, Scientific Data, 9 (2022), p. 361.

[34] K. Nalini, T. Lauvaux, C. Abdallah, J. Lian, P. Ciais, H. Utard, O. Laurent, and M. Ramonet, High-Resolution
Lagrangian Inverse Modeling of CO_2 Emissions Over the Paris Region During the First 2020 Lockdown Period, Journal of
Geophysical Research: Atmospheres, 127 (2022), p. e2021JD036032.

670   [35] G. M. L. NOAA, Trends in atmospheric carbon dioxide, annual mean growth rate for Mauna Loa, Hawaii.
https://gml.noaa.gov/ccgg/trends/gr.html [Accessed : June 2024].

[36] S. C. Pugliese, J. G. Murphy, F. R. Vogel, M. D. Moran, J. Zhang, Q. Zheng, C. A. Stroud, S. Ren, D. Worthy, and G.
Broquet, High-resolution quantification of atmospheric CO_2 mixing ratios in the Greater Toronto Area, Canada, July 2017.

[37] M. Ramonet, A. Chatterjee, P. Ciais, I. Levin, M. K. Sha, M. Steinbacher, and C. Sweeney, CO_2 in the Atmosphere:
675   Growth and Trends Since 1850, Oxford University Press, June 2023.

[38] A. A. Shusterman, V. E. Teige, A. J. Turner, C. Newman, J. Kim, and R. C. Cohen, The BErkeley Atmospheric CO_2
Observation Network: Initial evaluation, Atmospheric Chemistry and Physics, 16 (2016), pp. 13449–13463.

[39] J. Staufer, G. Broquet, F.-M. Bréon, V. Puygrenier, F. Chevallier, I. Xueref-Rémy, E. Dieudonné, M. Lopez, M.
Schmidt, M. Ramonet, O. Perrussel, C. Lac, L. Wu, and P. Ciais, The first 1-year-long estimate of the Paris region fossil fuel
680   CO_2 emissions based on atmospheric inversion, Atmospheric Chemistry and Physics, 16 (2016), pp. 14703–14726.

[40] P. P. Tans, A. M. Crotwell, and K. W. Thoning, Abundances of isotopologues and calibration of CO_2 greenhouse gas
measurements, Atmospheric Measurement Techniques, 10 (2017), pp. 2669–2685.

[41] Y. Té, P. Jeseck, B. Franco, E. Mahieu, N. Jones, C. Paton-Walsh, D. W. T. Griffith, R. R. Buchholz, J. Hadji-Lazaro,
D. Hurtmans, and C. Janssen, Seasonal variability of surface and column carbon monoxide over the megacity Paris, high-
685   altitude Jungfraujoch and Southern Hemispheric Wollongong stations, Atmospheric Chemistry and Physics, 16 (2016), pp.
10911–10925.

[42] K. R. Verhulst, A. Karion, J. Kim, P. K. Salameh, R. F. Keeling, S. Newman, J. Miller, C. Sloop, T. Pongetti, P. Rao, C.
Wong, F. M. Hopkins, V. Yadav, R. F. Weiss, R. M. Duren, and C. E. Miller, Carbon dioxide and methane measurements
from the Los Angeles Megacity Carbon Project – Part 1: Calibration, urban enhancements, and uncertainty estimates,
690   Atmospheric Chemistry and Physics, 17 (2017), pp. 8313–8341.

[43] I. Xueref-Remy, E. Dieudonné, C. Vuillemin, M. Lopez, C. Lac, M. Schmidt, M. Delmotte, F. Chevallier, F. Ravetta, O. Perrussel, P. Ciais, F.-M. Bréon, G. Broquet, M. Ramonet, T. G. Spain, and C. Ampe, Diurnal, synoptic and seasonal variability of atmospheric CO_2 in the Paris megacity area, Atmospheric Chemistry and Physics, 18 (2018), pp. 3335–3362.

[44] A. E. Yazidi, M. Ramonet, P. Ciais, G. Broquet, I. Pison, A. Abbaris, D. Brunner, S. Conil, M. Delmotte, F. Gheusi, F. Guerin, L. Hazan, N. Kachroudi, G. Kouvarakis, N. Mihalopoulos, L. Rivier, and D. Serça, Identification of spikes associated with local sources in continuous time series of atmospheric CO, CO_2 and CH_4, Atmos. Meas. Tech., (2018).

[45] C. Yver-Kwok, C. Philippon, P. Bergamaschi, T. Biermann, F. Calzolari, H. Chen, S. Conil, P. Cristofanelli, M. Delmotte, J. Hatakka, M. Heliasz, O. Hermansen, K. Komínková, D. Kubistin, N. Kumps, O. Laurent, T. Laurila, I. Lehner, J. Levula, M. Lindauer, M. Lopez, I. Mammarella, G. Manca, P. Marklund, J.-M. Metzger, M. Mölder, S. M. Platt, M. Ramonet, L. Rivier, B. Scheeren, M. K. Sha, P. Smith, M. Steinbacher, G. Vítková, and S. Wyss, Evaluation and optimization of ICOS atmosphere station data as part of the labeling process, Atmospheric Measurement Techniques, 14 (2021), pp. 89–116.

[46] C. L. Zhao and P. P. Tans, Estimating uncertainty of the WMO mole fraction scale for carbon dioxide in air, Journal of Geophysical Research : Atmospheres, 111 (2006), p. 2005JD006003.